Composites: Part A 185 (2024) 108358

Contents lists available at ScienceDirect

Composites Part A

journal homepage: www.elsevier.com/locate/compositesa

Processing and performance of ultra high temperature ceramic matrix composite (UHTCMCs) using radio frequency assisted chemical vapour infiltration (RF-CVI)

Vinothini Venkatachalam [a,*], Burkard Esser [b], Jon Binner [a,*]

[a] School of Metallurgy and Materials, University of Birmingham, B15 2SE, UK
[b] DLR, German Aerospace Center, Institute of Aerodynamics and Flow Technology, Linder Höhe, 51147 Cologne, Germany

ARTICLE INFO

Keywords:
Ultra high temperature ceramics (UHTCs) A
Carbon fibres A
Ceramic-matrix composites (CMCs) A
Permeability B
Computational modelling C
CT analysis D
Electron microscopy D
Chemical vapour infiltration (CVI) E

ABSTRACT

Ultra-high temperature ceramic matrix composites (UHTCMCs) have been produced using a radio frequency assisted chemical vapour infiltration (RF-CVI) process. The composites were based on 2.5D carbon fibre preforms with a 0 / 90° (out of plane) fibre orientation and containing 23 % fibre volume fraction. These were initially impregnated with zirconium diboride (ZrB_2) powder in the form of a slurry and then, after solvent removal, the majority of the porosity filled with pyrolytic carbon (PyC) using the RF-CVI process at 1273 K and 0.5 kPa chamber pressure. The latter resulted in a uniform rough laminar texture with good interfacial bonding. As intended, an inverse temperature profile was achieved using the RF heating, enabling uniform densification of the preform from the inside out, with no entrapped porosity and achieving 90 % of theoretical density in only 24 h, at least a tenfold reduction in processing time compared to the conventional CVI process and a fivefold reduction compared to other modified CVI processes such as forced flow or pressure gradient CVI. The resulting UHTCMCs displayed good mechanical strength and thermo-ablative behaviour.

1. Introduction

Next generation materials for space applications such as rocket nozzles and thermal protection systems for space vehicles flying at hypersonic speeds require materials to withstand a combination of extreme temperatures, chemically aggressive environments and rapid heating or cooling [1]. These demands are beyond the capabilities of current commercial engineering materials [2]. Ultra-high temperature ceramics (UHTC), composed primarily of metal diborides, are candidate materials for sharp leading edges on hypersonic re-entry vehicles [3]. The monolithic UHTC ceramic materials, however, display insufficient fracture toughness and hence thermal shock resistance for most potential applications and so have to be fibre reinforced to create ceramic matrix composites [4]. Carbon fibres (C_f) are generally preferred for their low density and cost combined with high stiffness and strength, and hence carbon fibre reinforced ultra-high temperature ceramic matrix composites (UHTCMCs) are now being widely investigated as high temperature structural materials for a variety of aerospace applications [5–7].

Although tremendous success has been achieved by the team from ISTEC, Italy, and Tecnalia, Spain, working within the C^3Harme programme [8–10], it is not simple to process UHTCMCs, especially those that do not also contain SiC, using conventional sintering techniques such as hot pressing and spark plasma sintering since they require very high sintering temperatures (>2273 K) that can result in damage to the fibres and/or grain growth of the matrix [7]. Since we aim for a maximum operating temperature of >2000 °C, the presence of SiC could lower significantly the ability to survive extreme conditions aimed for as SiC undergoes active oxidation and indeed can starts volatilizing above 1600 °C. Hence the present work specifically focused on Cf-ZrB_2 based composites without any SiC additions. Thus, an alternative approach was therefore to use non-sintering-based techniques such as chemical vapour infiltration (CVI) [11–13], reactive melt infiltration (RMI) [14,15] and precursor infiltration and pyrolysis (PIP) [16].

Chemical vapour infiltration is a leading technique for fabricating carbon / carbon (C/C) composites [17] and fibre-reinforced ceramic matrix composite materials, particularly silicon carbide / silicon carbide (SiC/SiC) composites [18,19]. The most common chemical reactions are the dissociation of methane and methyl trichlorosilane, respectively, both typically at around 1273 K.

* Corresponding authors.
E-mail addresses: V.Venkatachalam@bham.ac.uk (V. Venkatachalam), J.Binner@bham.ac.uk (J. Binner).

https://doi.org/10.1016/j.compositesa.2024.108358
Received 5 February 2024; Received in revised form 2 July 2024; Accepted 6 July 2024
Available online 7 July 2024

$$CH_4\ (g) + H_2\ (g) \rightarrow C\ (s) + 3H_2\ (g) \quad (1)$$

$$CH_3SiCl_3\ (l) + H_2\ (g) \rightarrow SiC\ (s) + 3HCl\ (g) + H_2\ (g) \quad (2)$$

Conventionally, the process is carried out under isothermal, isobaric conditions (I-CVI) and the process relies on the diffusion of the gases through the preform [17,20] followed by the deposition of the solid phase. Since the latter will typically occur wherever the preform is hottest and the concentration of the gases is highest, this means that deposition tends to occur first at the surfaces; this can lead to the formation of a 'crust' that subsequently blocks the channels and reduces the flow of the gases through the preform. This requires the process be stopped, the part(s) taken out and machined to remove the crust and then the whole process started again. To minimise this, the heating of the preform is extremely slow to try and achieve as uniform a temperature profile across it as possible and hence uniform densification [11,12]. This, plus the need for multiple (typically 2 or 3) machining steps, means that it is not uncommon for the industrial process to take several hundred hours (up to a thousand), spread over a period of 2–3 months. Attempts at using higher processing temperatures can result in the rate of chemical reaction exceeding the mass transfer of the reactant gases, which results in premature pore closure on the surface of the preforms, leaving entrapped porosity inside the parts [11,12].

In order to overcome these difficulties, various modifications have been carried out to the conventional CVI process, including [21,22]the use of thermal [20,23] and pressure gradients [24], or both [21,22] (the latter two cases are usually called "forced-flow CVI or F-CVI). A full description of the various versions may be found in [18,19]. As it appears from the surveys, most modified CVI processes require at least 120–150 h to make C/C composites.

To ensure a strong thermal gradient, a fluid filled CVI technique has been explored in increased deposition rates but it sometimes leads to mixed textures in the microstructure [25–27]. [18,19].

Volumetric heating using microwaves (for SiC_f preforms), or RF (for C_f preforms) can yield a stable inverted temperature profile since the combination of volume heating and surface heat losses lead to a higher temperature at the centre of the sample, at least if it has a suitable size [7,28–34]. This means that deposition occurs first at the centre, avoiding the 'crusting' that occurs with conventional I-CVI and building up the matrix from the centre-outwards. This provides the potential to achieve rapid densification of preforms, whilst, since the fundamental mechanism hasn't been changed, the crystallography and microstructure of the matrix remains the same as for I-CVI [13].

The goal of this work was to investigate the potential for making carbon fibre reinforced composite with ZrB_2 powder and pyro carbon matrices (C_f-ZrB_2-C_m) UHTCMCs using RF-CVI and then characterise their resulting properties to see if they have potential for use in applications such as thermal protection systems and rocket nozzles.

2. Experimental procedure

The primary starting materials were 2.5D continuous carbon fibre (C_f) preforms (23 vol% PAN C_f, Surface Transforms, Liverpool, UK) and zirconium diboride, ZrB_2, powder (HC Starck grade B, $d_{50} \sim 3$ μm, procured through ABCR GmbH & Co, Karlsruhe, Germany). The preforms consisted of layers of fabric stacked in an arrangement of random / 0° / random / 90° / random orientation, where 0° and 90° were unidirectional layers and the random layers were formed as a result of Surface Transform's needling process, as published elsewhere [13]. The ZrB_2 powder was turned into a 30 vol% slurry made using ethanol (AR grade, Fischer Scientific, Loughborough, UK) and containing 1 wt% of the dispersant polyethylene imine, PEI (linear, Avg Mn ~ 2500, PDI < 1.3, Sigma-Aldrich, Dorset, U.K). The slurry composition had previously been optimised to the required consistency, ~8 mPa.s at 100 s^{-1} shear rate [13].

The ZrB_2 slurry was introduced into the C_f preforms by manual injection using a 2.5 ml terumo syringe and 0.8 x 38 mm, 21G terumo agani needles (Medisupplies, Poole, U.K). The needles were inserted from the top to the bottom of the preform and then injection performed as the needle was withdrawn at a constant velocity and with a constant pressure on the syringe. Further details of the process have been provided elsewhere [35]. The distance between each injection had previously been optimised (for the 2.5D preforms) at 5 mm in both the x and y directions and the amount of slurry injected at each point was calculated with respect to the volume of the samples to achieve a final, dried density of ≥ 1.5 g cm^{-3}. After injection, the preforms were then dried in an oven in air at 348 K for 12 h (Genlab-MNO, Genlab Ltd, Cheshire, U.K). X-ray micro computed tomography, MicroCT (Skyscan2214, Bruker, Kontich, Belgium) and SEM analysis (JEOL 7000, Tokyo, Japan) was used to ensure that the slurry was distributed homogeneously throughout the samples and that a high powder content was achieved.

The ZrB_2 impregnated preforms were densified with pyrolytic carbon, PyC, using an RF EasyHeat induction furnace operating with 4.2 kW maximum power in the frequency range 150 – 400 kHz. Fig. 1 shows a schematic representation of the equipment and the target temperature was controlled using a two-colour pyrometer. Methane and hydrogen gases were used as the precursor gases and the key parameters such as the gas flow rate, ratio of methane to hydrogen and temperature were all determined experimentally to maximise the pyrolytic carbon deposition rate. To act as a benchmark and to aid in optimising the process conditions, equivalent samples were also produced using conventional I-CVI at Surface Transforms plc. in the UK.

Initially, the heat distribution from the coil used during the induction heating process was evaluated using a thermal imaging camera [36] and modelled using COMSOL Software [37,38].

With the combination of RF-heating, chamber pressure and gas flow conditions, an inverted temperature profile was established in the carbon preform containing ZrB_2 particles, resulting in the maximum temperature occurring in the centre of the sample; consequently, the reactant gas infiltration lead to carbon deposition being greater in the centre of the preform as compared to its periphery [4]. The PyC deposit phase formation and the crystallinity of the deposited carbon were examined using polarized light microscopy, PLM (Zeiss Axioplan 2 optical microscope, Oberkochen, Germany) and more quantitative analysis was undertaken using Raman spectroscopy (inVia Reflex, Reinshaw, New Mills, U.K). For the latter, the spot spectrum scanning was carried out at 50X magnification with a spot size of 1.5 μm and using a 514 nm green laser. The deposit thickness and final microstructures were characterized using further scanning electron microscopy (JEOL 7000) and microCT (Bruker Skyscan2214).

The micromechanical properties of the deposited carbon & fibres produced though RF-CVI were tested & compared against the conventional CVI process by mapping mechanical properties with high spatial resolution using arrays of nanoindentation data by Micromaterials U.K Ltd., Crewe. The nano indenter's integrated optical microscope was used to select test spots. Once the indenter was positioned, a 3D topographic image of the selected region was taken to determine the sample surface's suitability for nanoindentation. This was accomplished by scanning the sample perpendicular to the indenter with a nanometre-precision closed-loop piezoelectric scanner built into the sample stage. After this procedure, the indenter was kept against the sample surface ready to make indentation under a load of 1 μN via raising and lowering at various measurement points. The data from the piezo scanner and the indenter depth signal were combined to create a three-dimensional surface image. A grid of 1520 x 1 mN nanoindentation measurements were performed within the selected region. In addition, the results of nanoindentation were applied to a k-means clustering analysis [39] to determine statistical differences between the fibre and matrix phases.

A custom-built oxyacetylene torch (OAT) testing facility at University of Birmingham was used to thermo-ablatively assess the UHTCMCs [7 36].The graphite sample holders were used to hold the samples firmly using graphite screws. The samples of 62 × 20 × 17 mm sizes were

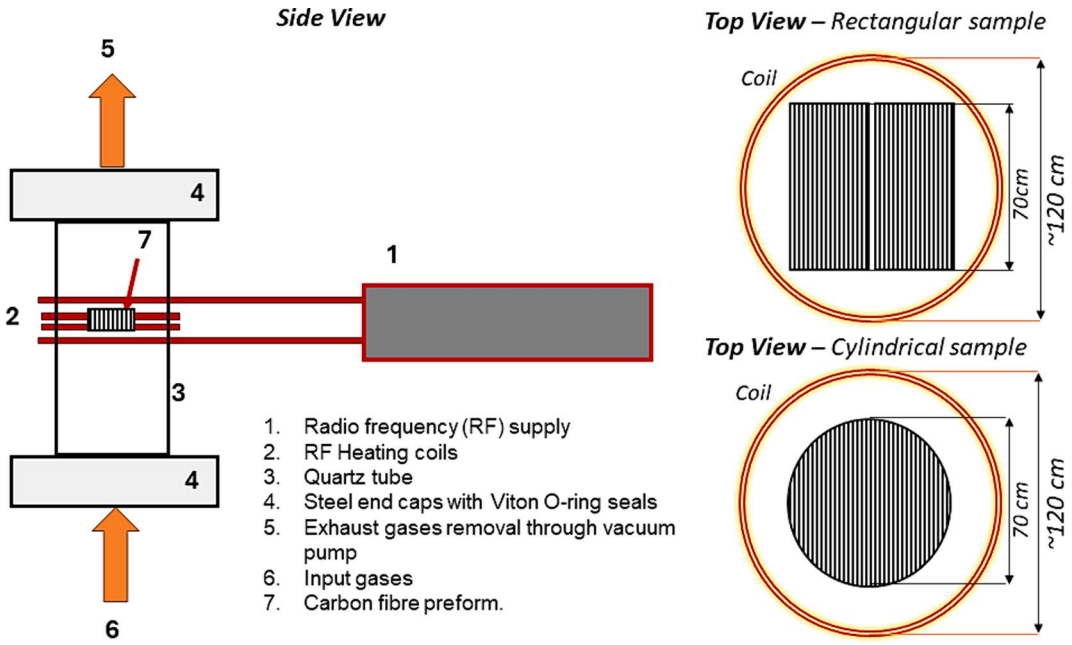

Fig. 1. Schematic diagram of the custom-built RF CVI set up at University of Birmingham.

rotated into the flame to provide a clear time-zero for every test and a standard set of conditions were used for all tests. This involved a heat flux of 0.6 MW m^{-2}, which was achieved using an oxidising flame with an acetylene: oxygen ratio of 1:1.35 and a set distance of 30 mm between the nozzle and the sample surface. Each sample was exposed to the torch flame for 60 s and a thermal imaging camera (FLIR A655sc, FLIR systems AB, Sweden) and two-colour pyrometer (METIS M3, Sensortherm, Germany) were used to monitor the sample surface temperature over time. Both the average mass and linear ablation rate of the samples were calculated from measurements obtained on each sample before and after testing. Further information on the oxyacetylene torch test has been provided elsewhere [35,36]. The ablated UHTCMCs surface profile was analysed using surface profile analyser (InfiniteFocus, Bruker Alicona imaging GmbH).

Further, stagnation tests were carried out by DLR using circular samples of 50 mm diameter and their arc-heated facility L3K in Cologne. L3K is constructed similarly to a traditional hypersonic blow-down wind tunnel, with the addition of a segmented arc-heater with a maximum electrical output of 6 MW, which enables the working gas to be energised to high enthalpy conditions. For thermal testing, samples were positioned in a convergent-divergent nozzle's homogeneous hypersonic free stream. This system allows thermal protection materials and structures to be evaluated under simulated re-entry conditions at flight-relevant heat fluxes and pressures and with a relevant chemical environment. Consequently, surface catalyticity and surface reactions are properly accounted for in the heat response of the specimens. The facilities at L3K are described in full in elsewhere [40,41]. The stagnation test was configured carefully to match the complete set of aerodynamic requirements being simulated. After baseline qualification tests were carried out at a heat flux rate of 2 MW/m^2 on three samples, two fresh samples were tested under more advanced conditions at a higher stagnation pressure of 718 hPa and heat flux of 8.5 MW/m^2. Further, to investigate these materials for reusability, one sample was exposed to a further three test runs, making four in total on the same sample.

3. Results and discussion

3.1. Characteristics of PyC

Before attempting full densification, it was necessary to characterize the deposited carbon material characteristics in the early stages. The carbon produced from the vapour phases consisted of a continuous carbon deposition over carbon fibres. Researchers have worked extensively on understanding the transition from smooth laminar to rough laminar (SL/RL) or smooth to regenerative (SL/ReL) conditions in the CVD/CVI process[42,43]. The anisotropy of RL and ReL, as indicated by their Ae and orientation angle (OA), is very similar, however, leading to confusion about the texture and structure of pyro carbon. Raman spectroscopy was employed to determine the structure of pyrocarbon by exploiting its sensitivity to structural defects, whilst optical polarised microscopy was used to measure the extinction angle for texture analysis [42–44]. The study was based on the identification of the 'Maltese cross', which is characteristic of laminar pyrolytic carbons, as well as their extinction angle, which is indicated by a 'bow tie'-like image. This effect is obtained by rotating the microscope analyser, which is initially positioned at 90 degrees to the angle required for the 'Maltese cross' extinction (Ae) [44,45]. The type of pyrolytic carbon has been characterised based on extinction angle as isotropic (<4°), dark laminar (DL); (4° < Ae < 12°), smooth laminar (SL) (12° <Ae < 18°), rough laminar (RL) (>18°) and regenerative laminar (ReL) (>22°) [46]. A rough laminar (RL) structure was desired since it provided both a high density and a high level of graphitization, which in turn yielded a high thermal conductivity [17] – useful for dissipating heat during its subsequent end-use. Although not directly needed for this application, an RL structure is also known to yield superior wear resistance, along with pseudo plastic failure behaviour [47,48]. Interestingly, the texture of the PyC deposited at 1273 K shows an extinction angle (Ae) of 18 – 21° measured using polarized light microscopy, PLM, as shown in Fig. 2, referring to the RL or ReL structures.

The primary surface of deposition was a prerequisite for producing well-oriented PyC layers [24,49]. Therefore, Raman spectroscopic analysis was used to analyse the structure of the pyro carbon deposition; it is a powerful and non-invasive tool used to investigate carbon based materials. It also reveals any disorder stacking in the graphene layers and the level of graphitisation, which is crucial for this end application. Consequently, Raman spectroscopy was used to investigate the deposited carbon at various stages of infiltration across the middle cross-section. Typically PyC shows two major peaks in the D (1360 cm^{-1}) and G (1580 cm^{-1}) bands. The D band represents the level of disorder in the graphene layers, whilst the G band provides information on the

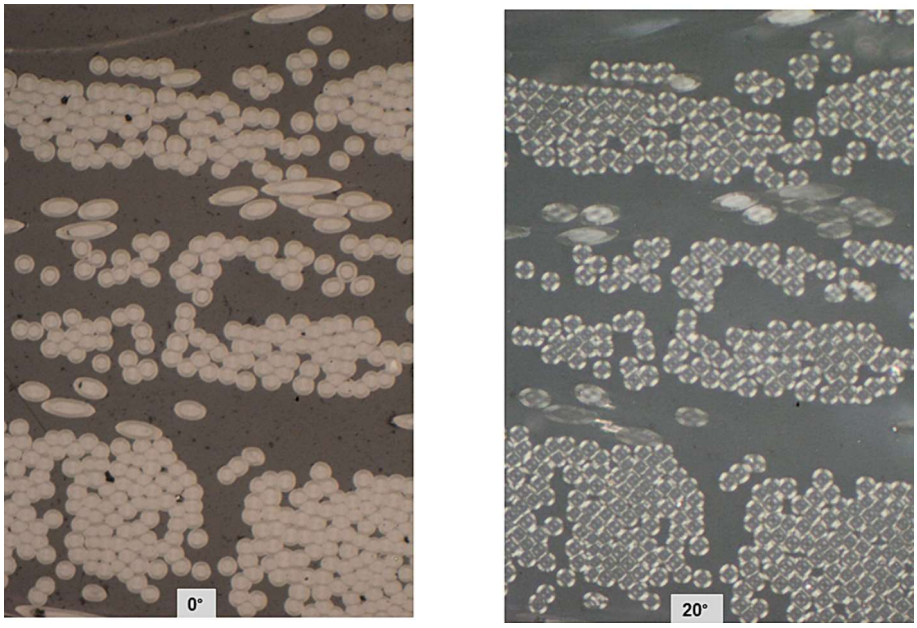

Fig. 2. Cross-polar optical micrographs of the pyrolytic carbon deposited using RF-CVI showing images at angles.

stretching of the C–C bonds in graphitic materials, i.e. it is correlated to the level of graphitisation present [50]. Also, the intensity ratio between the two bands (ID/IG) is inversely proportional to the degree of graphitisation [51]. Bourrat et al. [42] and Vallerot et al. [43] established a correlation between Raman peaks and pyrolytic carbon texture, so it is possible to extract information on layer stacking and crystallinity [48]. The findings strongly support the conclusion that the pyro carbon synthesised in this study, with an FWHMD (full width at half maximum) range of 75–137 and an extinction angle (Ae) of around 20, belonged to the rough laminar category of pyro carbon. The regenerative laminar shows a broad FWHM (>170) along with > 20 extinction angle.

Fig. 3 shows Raman data for a sample that had become ~75 % dense after 16 h of infiltration. The absence of a broad peak at 500 cm^{-1} confirms that the carbon deposit was of a crystalline nature. The intensity of the D band was strong on the carbon fibre (Cf), the PyC near the Cf and close to the ZrB_2 particles, whereas the intensity of the G band was stronger in the PyC deposited further away from the ZrB_2 particles. No significant change with D band intensities was observed, however, the full width at half maximum (FWHM) of the D band increased with

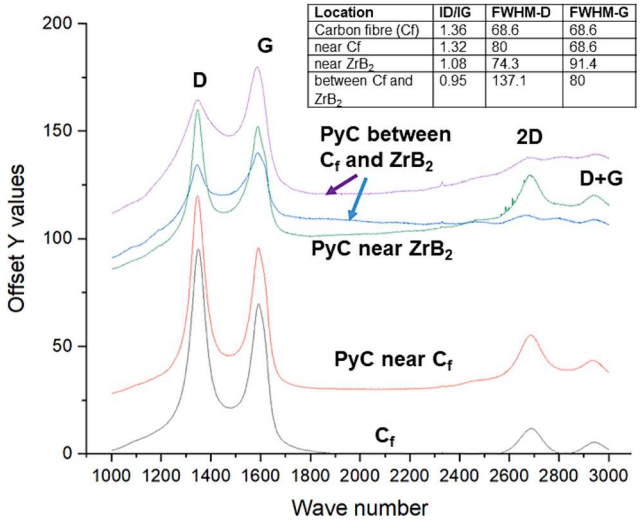

Fig. 3. Raman spectra of PyC deposited on the carbon preform with ZrB_2.

increasing distance away from the fibre and particles surfaces. This was expected, as higher deposition rates can cause the D band to expand as the rapidly growing structure can lead to a slight disordering of the layers. Additionally, sharp, intense, second-order (2D) bands at ~2650 cm^{-1} confirmed the presence of higher degree, three-dimensional (3D) ordering of graphene sheets [48]. There was no change in the intensities of the 2D band, which are attributed to orderliness and a lack of any stacking faults or rotational misalignment of the graphene sheets. Thus, the carbon deposition produced using RF-CVI retained a good in-plane structural ordering, which is also evident from the SEM microstrutures of the deposited PyC at various locations after 2 h of RF-CVI processing, Fig. 4. The structure of the PyC deposited was uniform along the radial directions of the carbon fibres and was fine grained and tightly stacked. In contrast, around the ZrB_2 particles the PyC deposited had a gradient structure of fine to coarse grains and was stacked in a relatively loose manner with a slight disorderly nature, correlating with the Raman data.

3.2. Deposition kinetics

Fig. 5a illustrates the rate of carbon deposition as a function of infiltration temperature; it is effectively the densification rate of the UHTCMCs. As can be seen, and as expected, the rate of densification increases with temperature. The CVI of PyC is a highly complex process that is driven by the rivalry between homogeneous reactions occurring in the gas phase and heterogeneous reactions occurring on the surface. The kinetics of CVI PyC growth follow the Arrhenius equation,

$$k = Aexp(-E_a)/(RT) \quad (3)$$

where k is the densification rate, T is the infiltration temperature, E_a is the activation energy, A is the frequency factor and R is the gas constant, 8.314 $Jmol^{-1}$ K^{-1}.

Fig. 5b shows the Arrhenius plot of the densification rate in the processing temperature range of 1173 K to 1273 K. The calculated activation energy extracted from the fitting curves are 36, 25 and 14 ± 2 $kJmol^{-1}$ $K^{-1}$for the deposition times of 2, 3 and 6 h respectively. These values are significantly lower than those previously reported in the literature for any recent advanced CVI modification methods such as thermal / pressure gradient, forced flow, etc. Since the lower activation energy results in a lower reaction barrier for PyC deposition, the densification rate for the RF-CVI technique is expected to be faster than

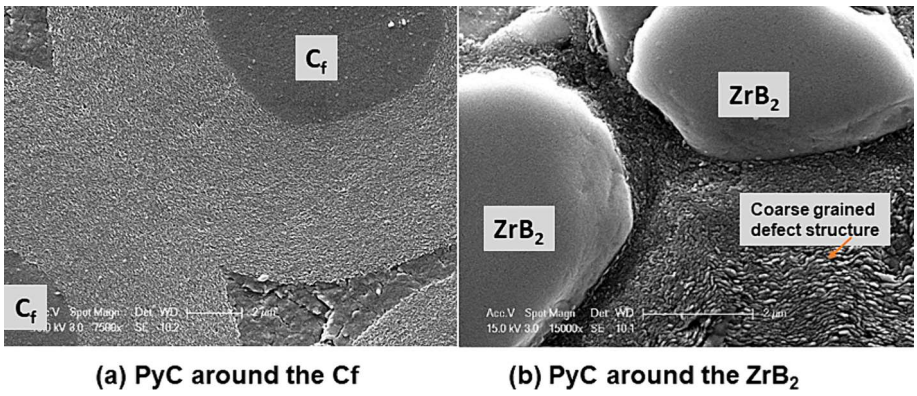

Fig. 4. SEM micrographs of the PyC deposition in the ZrB_2 loaded 2.5D carbon preform (a) adjacent to the carbon fibres, (b) adjacent to the ZrB_2 powder particles.

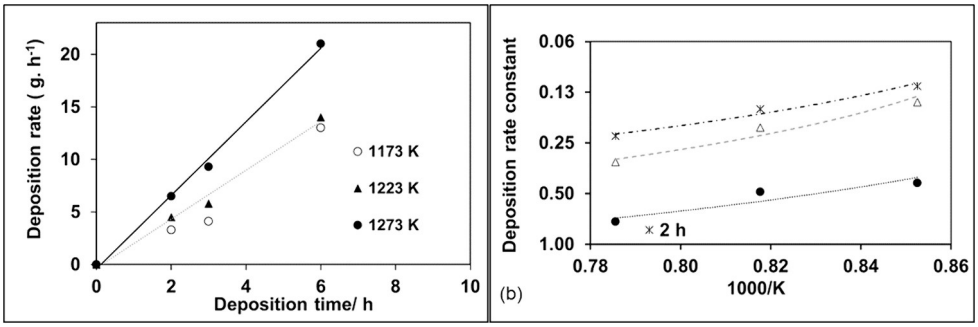

Fig. 5. (a) Amount of PyC deposited as a function of time at three different temperatures using RF-CVI, (b) Arrhenius plots of the deposition rate at different time.

that of any other CVI modified technique – as observed in practice. Interestingly, on the one hand, the average deposition rate decreases with deposition time, Fig. 5a, due to the infiltration front / concentration gradient of the reactant gases, thus reducing the deposition kinetics as explained by Vignoles et al.[23]. On the other hand, it is interesting that the calculated E_a value falls with deposition time, Fig. 5b, indicating the possibility of the deposition process accelerating as it progresses. Therefore, during the overall densification process, the rate of ultimate deposition remains fairly constant.

Fig. 6 shows a brief comparison chart of the activation energy values reported for PyC deposition through various CVI modifications at ≥ 1173 K. The values are comparable to the E-CVI [50] process on the strands of carbon fibres tows for 5 min (36.1 $kJmol^{-1}K^{-1}$) and the pressure gradient CVI for > 1313 K (43.2 $kJmol^{-1}K^{-1}$) [24].

Consequently, the reaction pathway would be similar to the E-CVI process [50], it's a very complex physico-chemical phenomena as there is an interplay between the diffusion of gases and the reaction kinetics along with infiltration front for the specific set up [30].

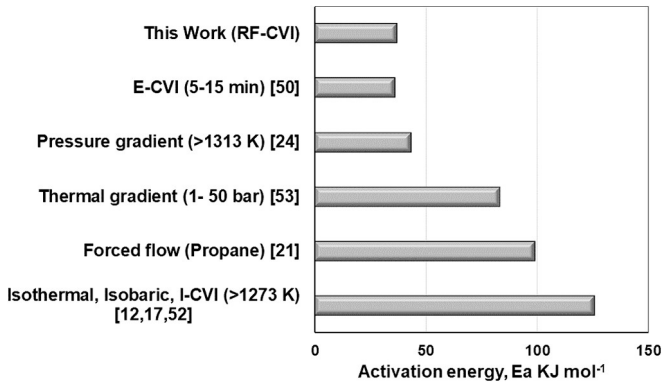

Fig. 6. A summary chart of reported activation energies of various PyC CVI processes.

Following the preliminary understanding developed from the carbon deposition and its characteristics, maximum densification was successfully achieved in just 24 h of infiltration with just 10 vol% remanent porosity. Therefore, the final composites thus contained ~ 58 ± 2 wt% ZrB_2 and ~ 27 ± 3 wt% pyrolytic carbon along with ~ 12 ± 1 wt% carbon fibre.[1] Consequently, UHTCMCs containing ZrB_2 powder and carbon matrices were consistently produced with bulk densities of 3.0 ± 0.2 g/cm^3 via RF-CVI in a processing time of 24 h. Further, it is evident from Fig. 7 that the PyC-densified 2.5D carbon preform, with ZrB_2 impregnation, contained ~ 20 % porosity after 16 h with the residual porosity being observed on the circumference of the preforms. Similarly, UHTC-impregnated carbon fibre preforms of both cylindrical and rectangular shapes, densified to ~ 90 % with PyC using RF CVI from the quantitative weight gain of the carbon preforms after infiltration shows a homogeneous distribution of the ZrB_2 from the micro-CT images, Fig. 8. A similar trend with respect to time was noticed for the samples densified using conventional CVI. Whilst taking up to 1000 h is typical in industry, the fastest approaches to achieving ~ 90 % density (around the maximum achievable by CVI) have been ~ 300 h for I-CVI [52 17 12] and 120 – 150 h via modified CVI processes such as force flow (F-CVI) [21], pressure gradient (P-CVI) [24] and thermal gradient (TG-CVI) [31], CVI. Previous work on RF-CVI have also shown that it is faster, though not as fast as in the current work, taking ~ 30 h to achieve partial densification of ~ 75 % for a 2.5 cm diameter carbon felt [3233,34]. Thus, provided the properties show that end-applications can live with ~ 10 % porosity in the final material, it means that RF-CVI can be used to produce UHTCMCs in reduced time and with reduced energy (and, therefore, one assumes, reduced costs).

[1] This is equivalent to 30 vol% ZrB_2, 23 vol% carbon fibre and 37 vol% pyrolytic carbon.

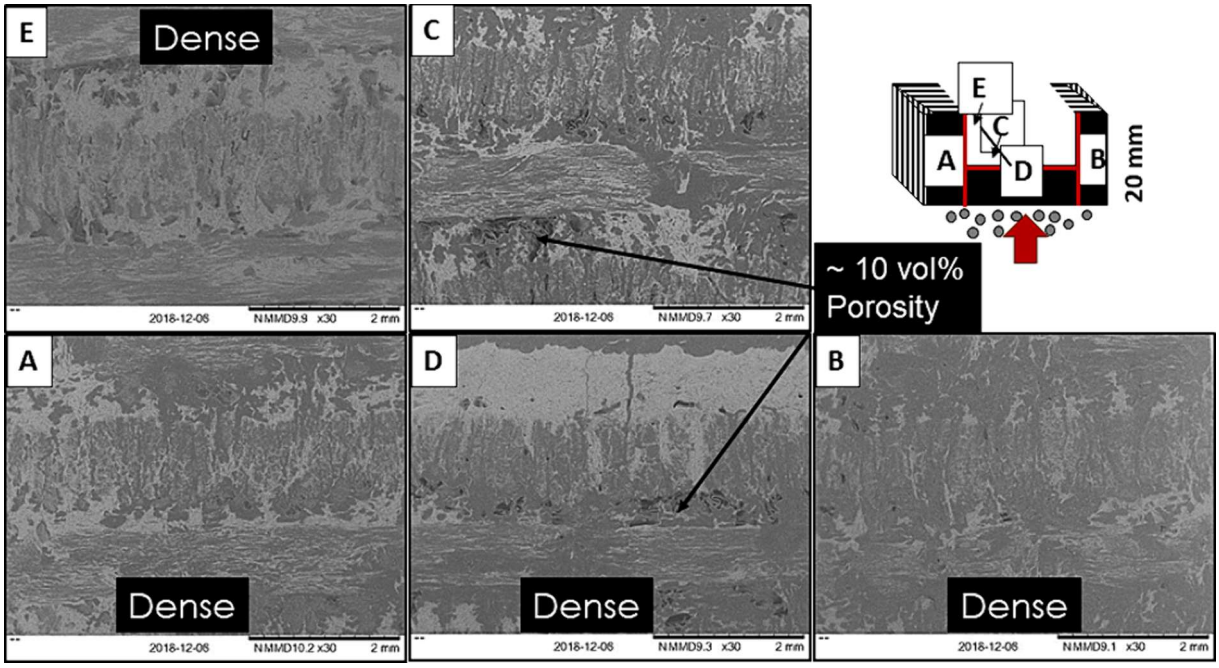

Fig. 7. SEM morphologies of PyC deposited on the ZrB_2 impregnated 2.5D carbon preform after 16 h.

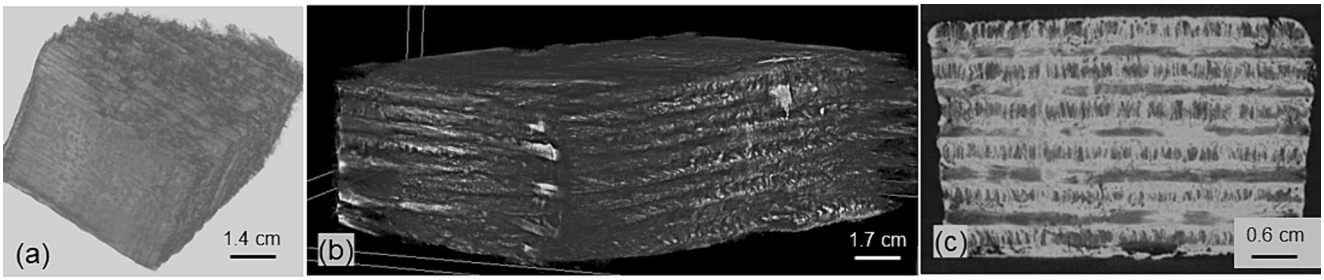

Fig. 8. X-ray tomography of the 2.5D carbon preforms impregnated with ZrB_2 and further densified by RF-CVI (a) Cylindrical sample, 50 mm diameter x 20 mm thickness, (b) Rectangular sample, 62 x 20 x 17 mm, (c) centre slice of sample b.

3.3. *Properties of the UHTCMCs*

(a) Nano mechanical behaviour of the carbon produced using RF-CVI

Even though a force of only 1 mN was used for the indenter, the force-penetration behaviour of fibres and matrix were quite different, with inelastic dissipation being observed in the CVI matrix but not the carbon fibres, whilst the unload curves were not elastic in either. Previously, only pure elastic responses were observed for most carbon-based materials when subjected to a higher load; 1 N for glassy carbon and 100 mN for pyrolytic carbon films [53,54]. Only highly oriented pyrolytic graphite (HPOG) exhibited conventional elastic–plastic behaviour when subjected to a small force of just 5 mN [55]. Recently, however, researchers have observed a similar pseudoplastic regime with a 10 mN load and a CVI-derived matrix [56]. Considering, the small load of only 1 mN utilised in the present study along with the fact that a high number of continuous test points were generated, a grid of 1520 nano-indentation measurements were performed within each selected region, the results have a higher spatial resolution compared to the literature

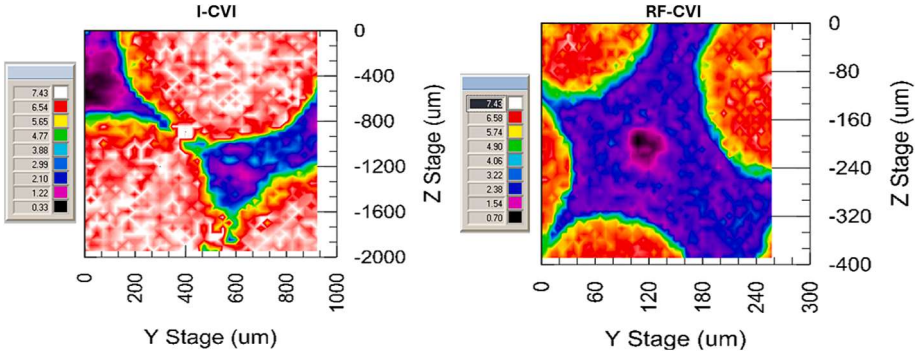

Fig. 9. Elastic modulus mapping of the PyC produced using (a) I-CVI and (b) RF-CVI.

values. This enabled the elastic and plastic work to be estimated for the test values. Fig. 9 shows the spatial mapping of the elastic modulus, along with the elastic and plastic work extracted from the data, for I-CVI and RF-CVI samples and Table 1 provides the effective elastic modulus of the CVI matrices. It can be seen that the elastic modulus of both the I-CVI and RF-CVI matrices matches with the reported values for pyrolytic carbon. Importantly, the elastic modulus of the PyC from RF-CVI matrices matches with the reported values of the rough laminar structures [54,57,58]. This confirms that the produced PyC structures match with standard I-CVI produced carbon matrices. Hardness is generally associated with resistance to plastic deformation, whereas Youngs modulus is associated with elasticity. Thus, the greater the effective Youngs modulus, the more elastic and stiffer the material. Consequently, the I-CVI fibres and matrices were found to be marginally stiffer than the equivalent RF-CVI fibres and matrices, however, considering the larger error bar for the I-CVI data compared to RF-CVI data, it is probably safer to say that they are essentially similar, as expected.

(b) Thermo-ablation testing – oxyacetylene torch (OAT) facility

From Fig. 10, it is clear that the sample surface reached a maximum temperature of ~2600 K in ~10 s and gradually headed towards a steady state condition after 30 s. The two-colour pyrometer gave an accurate surface temperature and was focused on the exact centre of the torch flame that was ablating the sample, whereas the infra-red thermal imaging camera was dependent on the emissivity of the material and recorded the whole sample surface, helping understanding of the heat distribution across the sample. The ZrB_2 in the UHTCMC matrix oxidised to ZrO_2 and B_2O_3 from ~ 700 °C, however the boria volatilized at > 1100 °C leading to a change in the emissivity of the materials surface. This was followed by an accelerated oxidation and a rise in surface temperature, as shown by the jump in temperature after ~ 30 s. Thus, the thin zirconium oxide layer formed remained intact, together with the boria liquid that survived up to ~ 1100 °C, then the zirconia started to sinter at > 1500 °C and provided a dense refractory layer protecting the fibers and the samples against further oxidation and ablation.

This resulted in a minimal mass ablation rate of 0.0017 g/s and a linear ablation rate of 0.0016 mm/s. Various literature ablation rates are tabulated in Table 2, however it is challenging to make useful comparisons due to the variation in sample surface temperatures achieved, along with missing data on heat flux and other parameters. In addition, most of the available data in the literature for similar matrices was either obtained from the use of ZrB_2 coatings[59,60] on carbon–carbon composites or from partial mixtures of ZrB_2 in polymeric matrices in carbon fabric composites [61,62], i.e. it is not of direct comparability to the present work. Therefore, plotting the values together doesn't make sense and hence is avoided here. Irrespective of the differences, however, it can be concluded that the mass and linear ablation rates obtained in the present work, even at the very high surface temperatures achieved, are minimal compared to most of the literature values for similar matrix compositions. As would be expected, the only equivalent performance was observed by Tang et. al.,[63] and was achieved using a similar approach but with the conventional chemical vapour infiltration technique (I-CVI).

(c) Thermo-ablation testing – Stagnation tests

Fig. 11 shows the thermal response of the UHTCMC sample that was tested four times consecutively using the arc-heating facility at DLR. The gas velocity was approximately 3500 ms^{-1} [64]. It shows the temperature / time curve for each cycle along with the erosion data and subsequent visual appearance of the sample. Differences in heating rate were observed only during the initial ~ 20 s for the first two cycles, thereafter the sample heated identically – and pretty much instantaneously – for the second two cycles. The formation of the oxide scale is visible after the first test cycle and, despite some minor spalling after the subsequent cycles, it remained intact and continued to provide the required protection from further ablation during the following cycles. It is also possible that it provided sufficient thermal insulation to cause the more rapid heating with the later heating runs. Each time, the sample surface attained a steady state condition of ~ 2600 K. These very promising results provide confidence regarding the materials produced via the RF-CVI process for reusable thermal protection systems.

3.4. Engineering values & cost analysis

Further, the UHTCMC technology developed at the University of Birmingham has been steadily moving up the technology readiness levels for a range of potential demanding applications.

1. As a part of an earlier MCM ITP programme[2] funded by Dstl, DGA and MBDA, a demonstrator jet vane of complex shape was designed, manufactured and satisfactorily tested, Fig. 12a, whilst in a related programme a large plate of roughly 30 × 30 × 10 cm was produced. The details were published elsewhere [4].
2. More recently, within the European Union-funded C3HARME programme, a range of parts, including rocket nozzle inserts, were produced as shown in Fig. 12b. They were tested under appropriate conditions using the excellent rocket nozzle testing facilities at the University of Naples in Italy and survived comfortably.

Historically, these UHT-CMCs have been considered complex and expensive materials however a recent analysis performed by QinetiQ[3] has indicated that they may not be as expensive as many imagine especially when made via the use of radio frequency assisted chemical vapour infiltration. The analysis suggested that manufacturing the jet vane shown in Fig. 12a could cost as little as about £70 ($90) [65]. Nevertheless, to reduce the cost of future UHT-CMC components that could be much larger, graded structures[66] could be used that mean that the UHTC phase is only present at the surface, which is exposed to extreme temperatures, whilst a more cost-effective CMC could be used inside the component. Work to this end has been satisfactorily completed and the gradation was such that there was no interface present.

Table 1
Effective elastic modulus values of the carbon matrices.

Material	E, GPa	Force	Reference
I-CVI	23.0 ± 8.7 (matrix) 62.3 ± 7.9 (fibres)	1 mN	*This work*
RF-CVI	17.6 ± 3.8 (matrix) 50.8 ± 5.5 (fibres)	1 mN	*This work*
Highly oriented pyrolytic graphite (HOPG)	15	5 mN	[55]
Glassy carbon	21	1 N	[53]
Rough laminar PyC(Parallel)	9–12	100	[54,57,58]
(Perpendicular)	18–19, 23 ± 1	mN	
Smooth laminar PyC	39	50 mN	[54]
Matrix on C/C composite	9.5	50 nN	[67]
Fibres parallel in C/C composite	13	50 mN	[54]
Fibres perpendicular in C/C composite	27	50 mN	[54]

[2] The Materials and Components for Missiles Innovation and Technology Partnership, MCM ITP, was a UK MoD and French DGA sponsored research fund open to all UK-French companies and academic institutions. Launched in 2007, the MCM ITP developed novel, exploitable technologies for generation- after-next missile systems until 2021 when it was replaced by the CW-ITP programme, see https://cwitp.com/.

[3] QinetiQ are a British centre of excellence in research and development, see https://www.qinetiq.com/en/.

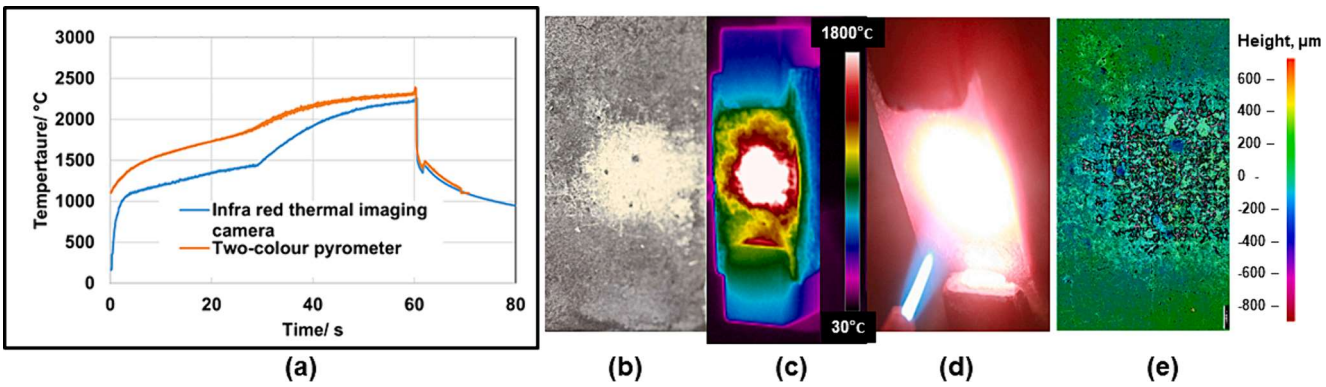

Fig. 10. (a) Temperature profiles during OAT testing, (b) Sample surface image after OAT test, (c) Thermal images from FLIR, (d) During the test, (e) Surface profile of the ablated surface.

Table 2
Ablation rate of the Cf/C-ZrB_2 composition materials.

Material	Surface Temperature, K	Mass ablation rate, MAR, g/s	Linear ablation rate, LAR, mm/s	Remarks	Referrence
Present work – 2.5DCf/ ZrB_2 + PyC	2600	0.0016	*0.0013*		
C/C –ZrB_2 composites produced via powder + ICVI	2073–2973	0.008–0.015	NA	The gas flows are different and linear ablation rate are missing	[63]
Nano ZrB_2 in C/C composites – cylinders	2493	NA	*0.0042*	Tested on the cylindrical samples to estimate the dimensional change.	[68]
7 % ZrB_2 in Cf/Phenolic composites	2273	NA	0.0029	The surface temperature profiles shows a continuous ablation and reaching a stable condition. Also, its importants for such highly volative materials to observed the mass loss which is missing in most of these materials.	[61]
4 % ZrB_2 in Cf/Novolac resin composite	773	12 % mass loss	0.0052	Surface temperature is too low to even compare.	[62]
La_2O_3-ZrB_2 coating on C/C composites	2270	~0.001	NA	Wedge shaped test sample	[59]
C/C-ZrB_2 coating	1773–1973	0.21–0.38	0.67–0.81	Low surface tempertaure and still high abation rate	[60]

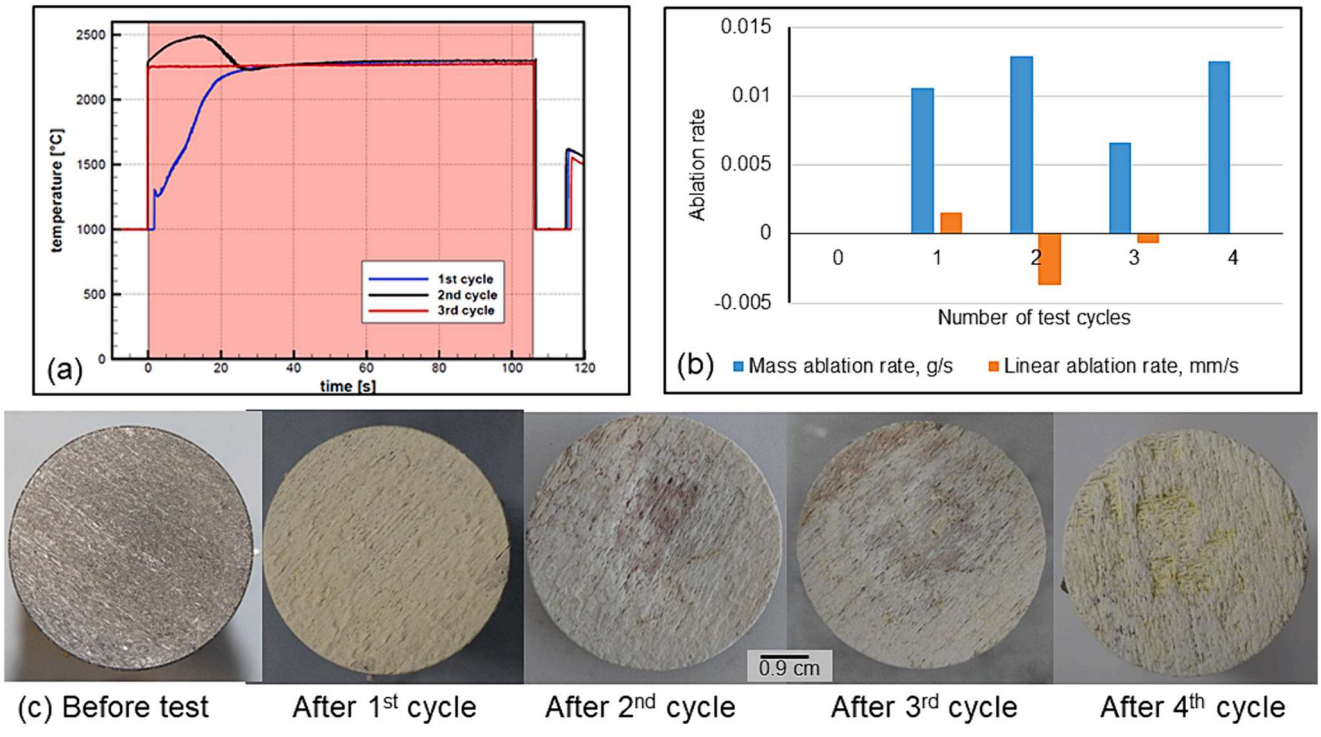

Fig. 11. (a) Temperature / time data for the stagnation tests, (b) Erosion data for the samples, (c) Sample surface images after each of 4 test cycles.

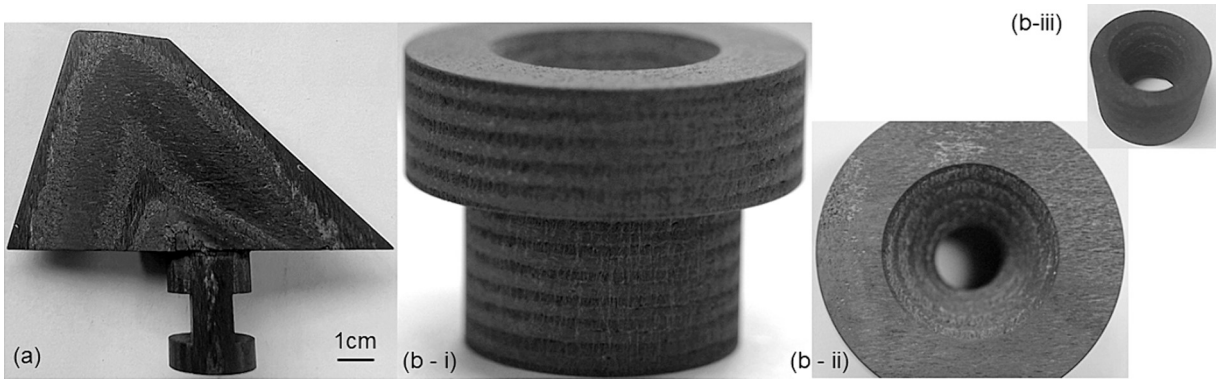

Fig. 12. A: a demonstrator jet vane, b: (i) side view & (ii) top view of the complete rocket nozzle, (iii) nozzle inserts.

4. Conclusions

We have successfully demonstrated an 'inside-out' thermal gradient process for the rapid densification using pyrolytic carbon of 2.5D carbon preforms prefilled with ~ 30 vol% of ZrB_2 powders via the use of radio frequency assisted chemical vapour infiltration (RF-CVI). Components can be produced in around 24 h, at least a tenfold reduction in processing time compared to the conventional CVI process and a fivefold reduction compared to other modified CVI processes. This opens up a new way of producing ultra-high temperature ceramic matrix composites (UHTCMCs) with low density ($\leq$3 g/cm^3) but which are capable of withstanding temperatures well above 2573 K combined with gas velocities ranging from subsonic to hypersonic. Samples even survived repeated testing to these conditions. Furthermore, the carbon deposits from the RF-CVI are comparable to those produced by conventional CVI. Finally, the UHTCMCs produced displayed excellent machinability and have been assessed as being much lower in cost than was anticipated.

CRediT authorship contribution statement

Vinothini Venkatachalam: Writing – review & editing, Writing – original draft, Visualization, Validation, Software, Methodology, Investigation, Formal analysis, Data curation, Conceptualization. **Burkard Esser:** Visualization, Validation, Resources, Methodology, Investigation, Formal analysis, Data curation. **Jon Binner:** Writing – review & editing, Supervision, Project administration, Funding acquisition, Conceptualization.

Declaration of competing interest

The authors declare that they have no known competing financial interests or personal relationships that could have appeared to influence the work reported in this paper.

Data availability

The data that has been used is confidential.

Acknowledgments

Most of this research work was financially funded by European Union's Horizon 2020 "Research and innovation programme" under grant agreement No 685594 (C3HARME). Other work was undertaken on related research programmes funded by the UK Government.

References

[1] Walker JD, Mueschke NJ, Chocron S. Hypersonics, advanced materials and shockwaves. Aerosp Am 2022;60.
[2] Bhat E by BN. Aerospace materials and applications / edited by Biliyar N. Bhat. 2018.
[3] Paul A, Binner J, Vaidhyanathan B. UHTC Composites for Hypersonic Applications. In: Fahrenholtz WG, Wuchina EJ, Lee WE, Zhou Y, editors. Ultra-High Temperature Ceramics, Hoboken, NJ: John Wiley & Sons, Inc; 2014, p. 144–66. Doi: 10.1002/9781118700853.ch7.
[4] Rubio V, Binner J, T Ackerman A, Cousinet S, Pommepuy N, Bertrand X. Ultra high temperature ceramic composite materials. Ultra-High Temperature Ceramics: Materials for Extreme Environment Applications IV 2017.
[5] Tang S, Hu C. Design, Preparation and properties of carbon fiber reinforced ultra-high temperature ceramic composites for aerospace applications: a review. J Mater Sci Technol 2017;33:117–30. https://doi.org/10.1016/j.jmst.2016.08.004.
[6] Sciti D, Zoli L, Silvestroni L, Cecere A, Di Martino GD, Savino R. Design, fabrication and high velocity oxy-fuel torch tests of a Cf-ZrB_2- fiber nozzle to evaluate its potential in rocket motors. Mater Des 2016;109:709–17. https://doi.org/10.1016/j.matdes.2016.07.090.
[7] Binner J, Porter M, Baker B, Zou J, Venkatachalam V, Diaz VR, et al. Selection, processing, properties and applications of ultra-high temperature ceramic matrix composites, UHTCMCs – a review. Int Mater Rev 2019:1–56. https://doi.org/10.1080/09506608.2019.1652006.
[8] Mungiguerra S, Di Martino GD, Cecere A, Savino R, Zoli L, Silvestroni L, et al. Ultra-high-temperature testing of sintered ZrB_2-based ceramic composites in atmospheric re-entry environment. Int J Heat Mass Transf 2020;156:119910. https://doi.org/Doi: 10.1016/j.ijheatmasstransfer.2020.119910.
[9] Sciti D, Zoli L, Vinci A, Silvestroni L, Mungiguerra S, Galizia P. Effect of PAN-based and pitch-based carbon fibres on microstructure and properties of continuous Cf/ZrB_2-SiC UHTCMCs. J Eur Ceram Soc 2020. https://doi.org/10.1016/j.jeurceramsoc.2020.05.032.
[10] Vinci A, Zoli L, Galizia P, Kütemeyer M, Koch D, Sciti D. Reactive melt in\filtration of carbon fibre reinforced ZrB2/B composites with Zr_2Cu. Compos Part A Appl Sci Manuf 2020:105973. https://doi.org/Doi: 10.1016/j.compositesa.2020.105973.
[11] Naslain R, Langlais F, Fedou R. The CVI-processing of ceramic matrix composites. Le Journal de Physique Colloques 1989. https://doi.org/10.1051/jphyscol:1989526.
[12] Lazzeri A. CVI Processing of Ceramic Matrix Composites. Ceramics and Composites Processing Methods, Hoboken, NJ, USA: John Wiley & Sons, Inc.; 2012, p. 313–49. Doi: 10.1002/9781118176665.ch9.
[13] Rubio V, Binner J, Cousinet S, Le Page G, Ackerman T, Hussain A, et al. Materials characterisation and mechanical properties of C_f-UHTC powder composites. J Eur Ceram Soc 2019;39:813–24. https://doi.org/10.1016/j.jeurceramsoc.2018.12.043.
[14] Hillig WB. Melt Infiltration Approach to Ceramic Matrix Composites. J Am Ceram Soc 1988. https://doi.org/10.1111/j.1151-2916.1988.tb05840.x.
[15] Kütemeyer M, Schomer L, Helmreich T, Rosiwal S, Koch D. Fabrication of ultra high temperature ceramic matrix composites using a reactive melt infiltration process. J Eur Ceram Soc 2016;36:3647–55. https://doi.org/10.1016/j.jeurceramsoc.2016.04.039.
[16] Yan C, Liu R, Zha B, Zhang C. Fabrication and properties of 3-dimensional 4-directional C_f/HfC-SiC composites by precursor impregnation and pyrolysis process. J Alloy Compd 2018;739:955–60. https://doi.org/10.1016/j.jallcom.2017.12.059.
[17] Delhaes P. Chemical vapor deposition and infiltration processes of carbon materials. Carbon N Y 2002;40:641–57. https://doi.org/10.1016/S0008-6223(01)00195-6.
[18] Vignoles GL. Chemical vapor deposition/infiltration processes for ceramic composites. Adv Compos Manufact Process Des 2015:147–76. https://doi.org/10.1016/B978-1-78242-307-2.00008-7.
[19] Kopeliovich D. Advances in manufacture of ceramic matrix composites by infiltration techniques. Adv Ceram Matrix Compos: Second Edition 2018:93–119. https://doi.org/10.1016/B978-0-08-102166-8.00005-0.
[20] Golecki I. Rapid vapor-phase densification of refractory composites. Mater Sci Eng R-Rep 1997;20:37–124.

[21] Vaidyaraman S, Lackey WJ, Agrawal PK, Miller MA. Carbon/carbon processing by forced flow-thermal gradient chemical vapor infiltration using propylene. Carbon N Y 1996;34:347–62. https://doi.org/10.1016/0008-6223(95)00190-5.

[22] Roman YG. Forced flow chemical vapour infiltration. 1994. Doi: 10.6100/IR418123.

[23] Vignoles GL, Descamps C, Charles C, Klein C. How is it possible to get optimal infiltration fronts during chemical vapor infiltration with thermal gradients ? Open Ceram. 2023;15:100375. https://doi.org/10.1016/J.OCERAM.2023.100375.

[24] Xia LH, Huang BY, Zhang FQ, Jin L, Chen D, Tang Q. Rapid Densification of Carbon/Carbon Composites Plate by Pressure-Gradient Chemical Vapor Infiltration. Adv Eng Mater 2017;19. Doi: 10.1002/adem.201600329.

[25] dos Santos JJS, Regiani I. Fast densification process in manufacturing carbon/carbon using vegetable precursors. J Aerosp Technol Manage 2018. https://doi.org/10.5028/jatm.v10.921.

[26] Rovillain D, Trinquecoste M, Bruneton E, Derré A, David P, Delhaès P. Film boiling chemical vapor infiltration: An experimental study on carbon/carbon composite materials. Carbon (New York) 2001;39:1355–65.

[27] Vignoles GL, Goyhénèche J-M, Sébastian P, Puiggali J-R, Lines J-F, Lachaud J, et al. The film-boiling densification process for C/C composite fabrication: From local scale to overall optimization. Chem Eng Sci 2006;61:5636–53.

[28] Yin Y, Binner J, Cross T. Microwave assisted chemical vapor infiltration for ceramic matrix composites. Microwaves: Theory Appl Mater Process IV, 1997, p. 349–56.

[29] Matthew Porter Binner J. Page 1 of 1 High Temperature Composites Using Microwave Enhanced Chemical Vapor Infiltration FORM SF 298 Page 1 of 1 REPORT DOCUMENTATION PAGE. University of Birmingham; 2020.

[30] Leutard D, Vignoles GL, Lamouroux F, Bernard B. Monitoring density and temperature in C/C composites processing by CVI with induction heating. vol. 9. 2001. Doi: 10.1023/A:1015251518333.

[31] Vignoles GL, Maillé L, Talué G, Badey Q, Guette A, Pailler R, et al. Chemical supercritical fluid infiltration of pyrocarbon with thermal gradients: deposition kinetics and multiphysics modeling. J Compos Sci 2022:6. https://doi.org/10.3390/jcs6010020.

[32] Devlin DJ, Barbero RS, KS. Radio frequency assisted chemical vapor infiltration. In: International conference; 13th, Chemical vapor deposition; 1996; Los Angeles; CA in PROCEEDINGS- ELECTROCHEMICAL SOCIETY PV ; 96/5 ; 571-578, vol. 96/5, 1996, p. 571–8.

[33] Vikas M, ED J. Effect of Geometry on CVI with RF Heating. In: 22nd Annual Conference on Composites, Advanced Ceramics, Materials, and Structures: B: Ceramic Engineering and Science Proceedings, Wiley-Blackwell; 2010, p. 526–34. Doi: 10.1002/9780470294499.ch61.

[34] Midha V, Economou DJ. Radio frequency heating benefits. PSC Litzler Company 2016;144:4062–71.

[35] Baker B, Rubio V, Ramanujam P, Binner J, Hussain A, Ackerman T, et al. Development of a slurry injection technique for continuous fibre ultra-high temperature ceramic matrix composites. J Eur Ceram Soc 2019;39:3927–37. https://doi.org/10.1016/j.jeurceramsoc.2019.05.070.

[36] Paul A, Venugopal S, Binner JGP, Vaidhyanathan B, Heaton ACJ, Brown PM. UHTC–carbon fibre composites: preparation, oxyacetylene torch testing and characterisation. J Eur Ceram Soc 2013;33:423–32. https://doi.org/10.1016/J.JEURCERAMSOC.2012.08.018.

[37] Istardi D, Triwinarko A. Induction heating process design using comsol® multiphysics software. Telkomnika 2011;9:327–34. https://doi.org/10.12928/telkomnika.v9i2.704.

[38] K. Djellabi MEHL. Induction heating process design using comsol® multiphysics software Version 4.2a. Int J Electr Comput Energetic Electron Commun Eng 2014;8:72–5. Doi: 10.12928/telkomnika.v9i2.704.

[39] Marx DT, Riester L. Mechanical properties of carbon—carbon composite components determined using nanoindentation. Carbon N Y 1999;37:1679–84. https://doi.org/10.1016/S0008-6223(98)00239-5.

[40] Gülhan A, Esser B. Arc-Heated Facilities as a Tool to Study Aerothermodynamic Problems of Reentry Vehicles. Advanced Hypersonic Test Facilities, Reston, VA: American Institute of Aeronautics and Astronautics; 2002, p. 375–403. Doi: 10.2514/5.9781600866678.0375.0403.

[41] Gülhan A, Esser B, Koch U. Experimental investigation of reentry vehicle aerothermodynamic problems in arc-heated facilities. J Spacecr Rockets 2001;38:199–206. https://doi.org/10.2514/2.3670.

[42] Bourrat X, Langlais F, Chollon G, Vignoles GL. Low temperature pyrocarbons: A review. J Braz Chem Soc, vol. 17, Sociedade Brasileira de Quimica; 2006, p. 1090–5. Doi: 10.1590/S0103-50532006000600005.

[43] Vallerot JM, Bourrat X, Mouchon A, Chollon G. Quantitative structural and textural assessment of laminar pyrocarbons through Raman spectroscopy, electron diffraction and few other techniques. Carbon N Y 2006;44:1833–44. https://doi.org/10.1016/j.carbon.2005.12.029.

[44] Gray RJ, Cathcart JV. Polarized light microscopy of pyrolytic carbon deposits. J Nucl Mater 1966;19:81–9. https://doi.org/10.1016/0022-3115(66)90133-4.

[45] Lamouroux F, Bertrand S, Pailler R, Naslain R, Cataldi M. ceramic-matrix composites 1999;59:1073–85.

[46] Bourrat X, Fillion A, Naslain R, Chollon G, Brendlé M. Regenerative laminar pyrocarbon. Carbon (New York) 2002;40:2931–45.

[47] Pierson HO, Northrop DA. Carbon-felt, carbon-matrix composites: dependence of thermal and mechanical properties on fiber precursor and matrix structure. J Compos Mater 1975;9:118–37. https://doi.org/10.1177/002199837500900203.

[48] Zhang WG, Hüttinger KJ. Densification of a 2D carbon fiber preform by isothermal, isobaric CVI: kinetics and carbon microstructure. Carbon N Y 2003;41:2325–37. https://doi.org/10.1016/S0008-6223(03)00284-7.

[49] Vignoles GL, Duclous R, Gaillard S. Analytical stability study of the densification front in carbon- or ceramic-matrix composites processing by TG-CVI. Chem Eng Sci 2007;62:6081–9. https://doi.org/10.1016/j.ces.2007.06.022.

[50] Hu C, Zhao R, Ali S, Wang Y, Pang S, Li J, et al. Deposition kinetics and mechanism of pyrocarbon for electromagnetic-coupling chemical vapor infiltration process. J Mater Sci Technol 2022;101:118–27. https://doi.org/10.1016/j.jmst.2021.06.020.

[51] Wang T, Li H, Shen Q, Li K, Li W, Song Q, et al. Dependence of mechanical properties on microstructure of high-textured pyrocarbon prepared via isothermal and thermal gradient chemical vapor infiltration. Compos B Eng 2020;192:107982. https://doi.org/10.1016/j.compositesb.2020.107982.

[52] Rubio V, Ramanujam P, Binner J. Ultra-high temperature ceramic composite. Adv Appl Ceram 2018;117:s56–61. https://doi.org/10.1080/17436753.2018.1475140.

[53] Iwashita N, Field JS, Swain MV. Indentation hysteresis of glassy carbon materials. Philos. Mag. A: Phys. Condens. Matter Struct. Defects Mech. Propert. 2002;82:1873–81. https://doi.org/10.1080/01418610208235699.

[54] Diss P, Lamon J, Carpentier L, Loubet JL, Kapsa P. Sharp indentation behavior of carbon/carbon composites and varieties of carbon. Carbon N Y 2002;40:2567–79. https://doi.org/10.1016/S0008-6223(02)00169-0.

[55] Xiao J, Zhang L, Zhou K, Li J, Xie X, Li Z. Anisotropic friction behaviour of highly oriented pyrolytic graphite. Carbon N Y 2013;65:53–62. https://doi.org/10.1016/J.CARBON.2013.07.101.

[56] Mohammed ASK, Sehitoglu H, Rateick R. Interface graphitization of carbon-carbon composites by nanoindentation. Carbon N Y 2019;150:425–35. https://doi.org/10.1016/J.CARBON.2019.05.038.

[57] Leyssale JM, Couégnat G, Jouannigot S, Vignoles GL. Mechanisms of elastic softening in highly anisotropic carbons under in-plane compression/indentation. Carbon N Y 2022;197:425–34. https://doi.org/10.1016/j.carbon.2022.06.063.

[58] Rollin M, Jouannigot S, Lamon J, Pailler R. Characterization of fibre/matrix interfaces in carbon/carbon composites. Special Issue on the 12th European Conference on Composite Materials, ECCM 2006, vol. 69, European Society for Composite Materials; 2009, p. 1442–6. Doi: 10.1016/j.compscitech.2008.09.023.

[59] Li B, Li H, Yao X, Chen Y, Hu X, Feng G, et al. Ablation behavior of sharp leading edge parts made of rare earth La-compound modified ZrB2 coated C/C composites. Corros Sci 2020;175:108895. https://doi.org/10.1016/J.CORSCI.2020.108895.

[60] Xu B, He R, Hong C, Ma Y, Wen W, Li H, et al. Ablation behavior and mechanism of double-layer ZrB2-based ceramic coating for lightweight carbon-bonded carbon fiber composites under oxyacetylene flame at elevate temperature. J Alloy Compd 2017;702:551–60. https://doi.org/10.1016/J.JALLCOM.2017.01.242.

[61] Amirsardari Z, Aghdam RM, Salavati-Niasari M, Shakhesi S. Preparation and characterization of nanoscale ZrB2/carbon-resol composite for protection against high-temperature corrosion. J Therm Anal Calorim 2015;120:1535–41. https://doi.org/10.1007/s10973-015-4474-7.

[62] Amirsardari Z, Aghdam RM. Comparison of weight-loss changes with different compositions of ZrB2 nanoparticles in carbon fabric-novolac composite at high temperature. Micro Nano Lett 2017;12:589–94. https://doi.org/10.1049/mnl.2017.0071.

[63] Tang S, Deng J, Wang S, Liu W, Yang K. Ablation behaviors of ultra-high temperature ceramic composites. Mater Sci Eng A 2007;465:1–7. https://doi.org/10.1016/J.MSEA.2007.02.040.

[64] Gülhan A, Esser B, Koch U, Fischer M, Magens E, Hannemann V. Characterization of high-enthalpy-flow environment for ablation material tests using advanced diagnostics. AIAA J 2018;56:1072–84. https://doi.org/10.2514/1.J056312.

[65] Healey A & Greenwood J. Cost analysis of Cf-ZrB_2 prototype jet vane (private communication). 2022.

[66] Silvestroni L, Capiani C, Dalle Fabbriche D, Melandri C. Novel light and tough ZrB2-based functionally graded ceramics. Compos B Eng 2016;99:321–9. https://doi.org/10.1016/J.COMPOSITESB.2016.06.001.

[67] Hao MY, Luo RY, Xiang Q, Hou ZH, Yang W, Shang HD. Effects of fiber-type on the microstructure and mechanical properties of carbon/carbon composites. Xinxing Tan Cailiao/New Carbon Materials 2014;29:444–53. https://doi.org/10.1016/S1872-5805(14)60149-9.

[68] Jayaseelan DD, de Sá RG, Brown P, Lee WE. Reactive infiltration processing (RIP) of ultra high temperature ceramics (UHTC) into porous C/C composite tubes. J Eur Ceram Soc 2011;31:361–8. https://doi.org/10.1016/j.jeurceramsoc.2010.10.013.